

**Theoretical model for seawater and sea sand concrete-filled circular FRP tubular stub  
columns under axial compression**

Y.L. Li<sup>a</sup>, J.G. Teng<sup>b</sup>, X.L. Zhao<sup>a\*</sup> and R.K. Singh Raman<sup>c,d</sup>

(\*corresponding author: [ZXL@monash.edu](mailto:ZXL@monash.edu))

<sup>a</sup> Department of Civil Engineering, Monash University, Clayton, VIC 3800, Australia

<sup>b</sup> Department of Civil and Environmental Engineering, The Hong Kong Polytechnic University,  
Hong Kong, China

<sup>c</sup> Department of Mechanical and Aerospace Engineering, Monash University, Clayton, VIC 3800,  
Australia

<sup>d</sup> Department of Chemical Engineering, Monash University, Clayton, VIC 3800, Australia

**ABSTRACT**

The use of FRP with seawater and sea sand concrete (SWSSC) holds great potential for marine and coastal infrastructure, and concrete-filled FRP tubular columns are among the attractive forms of structural members for such applications. This paper presents a theoretical model for the compressive behaviour of seawater and sea sand concrete-filled circular FRP tubular stub columns. FRP tubes can be manufactured to possess considerable strength and stiffness in the longitudinal direction, so the behaviour of concrete-filled FRP tubes differed substantially from that of concrete columns with an FRP wrap (also referred to as “concrete-filled FRP wraps”) which commonly contains fibres only in the hoop direction. Many theoretical models have been proposed for concrete-filled FRP wraps, but very limited work has been conducted on the theoretical modelling of concrete-filled FRP tubes. In the present study, an existing dilation model for concrete-filled FRP wraps is combined with a biaxial stress analysis of the FRP tube so that the effect of the Poisson’s ratio of the FRP tube is properly accounted for. In order to predict the buckling of the FRP tube, a maximum strain buckling failure

criterion is proposed and is shown to be in reasonable agreement with the experimental results. Moreover, the load carried by the FRP tube is studied, and a simplified model is proposed to determine the load shared by the FRP tube during the entire loading process. Finally, a theoretical model for SWSSC-filled FRP tubular columns is proposed, in which the behaviour of both the concrete and the FRP tube as well as their interactions are explicitly modelled (i.e., an analysis-oriented model). The proposed model gives reasonably close predictions of the existing experimental data.

## KEYWORDS

Concrete-filled FRP tube, confinement, dilation, theoretical model, seawater and sea sand concrete, axial compression

## NOMENCLATURE

$A_c$	=	cross-sectional area of concrete
$A_f$	=	cross-sectional area of FRP tube
$D_i$	=	diameter of concrete core ( $=D_o-2t_o$ )
$D_o$	=	outer diameter of FRP tube
$E_c$	=	elastic modulus of unconfined concrete
$E_h$	=	elastic modulus of FRP tube in hoop direction
$E_{hsec}$	=	secant modulus of FRP tube in hoop direction
$E_l$	=	elastic modulus of FRP tube in longitudinal direction
$f_{co}$	=	unconfined concrete strength
$f^*$	=	peak stress of confined concrete
$cc$	=	confining pressure
$f_l$	=	hoop tensile strength of FRP tube (by split-disk test)
$f_{uh}$	=	longitudinal compressive strength of FRP tube (by compressive test on short tube)
$f_{ul,c}$	=	longitudinal tensile strength of FRP tube (by tensile coupon test)
$f_{ul,t}$	=	number of incremental steps
$I$	=	factor 1
$k_1$	=	factor 2
$k_2$	=	factor 3
$k_3$	=	load carried by column
$N$	=	load carried by FRP tube
$N_f$	=	ultimate load of FRP tube
$N_{fu}$	=	

$N_t$	=	experimental ultimate load
$t_o$	=	thickness of FRP tube
$\Delta\epsilon_h$	=	hoop strain increment
$\epsilon_c$	=	axial strain
$\epsilon_{c,SG}$	=	axial strain (from strain gauge)
$\epsilon_{cb}$	=	axial strain at tube buckling (predicted)
$\epsilon_{cb,t}$	=	axial strain at tube buckling (experiment)
$\epsilon^*$		
$\epsilon_{cc}$	=	axial strain at confined concrete peak stress $f'^*_{cc}$
$\epsilon_{co}$	=	axial strain at unconfined concrete strength $f'_c$
$\epsilon_{cu}$	=	ultimate axial strain
$\epsilon_{fu}$	=	axial strain at ultimate load of FRP tube $N_{fu}$
$\epsilon_h$	=	hoop strain
$\epsilon_{hb}$	=	hoop strain at tube buckling
$\epsilon_{hu}$	=	ultimate hoop strain of FRP tube
$\epsilon_l$	=	longitudinal strain in FRP tube
$\epsilon_{lat}$	=	lateral strain
$\eta$	=	reduction factor for FRP tube
$\rho_K$	=	confinement stiffness
$\sigma_h$	=	hoop stress in FRP tube
$\sigma_l$	=	longitudinal stress in FRP tube
$\nu_h$	=	Poisson's ratio (hoop tension)
$\nu_l$	=	Poisson's ratio (longitudinal compression)

## 1. INTRODUCTION

In recent decades, fiber reinforced polymer (FRP) has been increasingly used in civil engineering due to its high strength-to-weight ratio and desirable durability performance. One of the applications is in concrete-filled FRP tubular members, in which the FRP tube, with appropriate fibre orientations, can be used to provide strength and stiffness in both the longitudinal and the hoop directions. In such columns, the FRP tube acts as the stay-in-place formwork for concrete casting and provides confinement to the core concrete to enhance its strength and ductility, in addition to serving as the longitudinal and shear reinforcement [1, 2]. Due to the absence of steel in such columns, seawater and sea sand concrete (SWSSC) can be used instead of ordinary concrete, leading to FRP-SWSSC hybrid systems, an attractive concept with great potential that was first proposed by the second author for marine and coastal infrastructure [3, 4]. The usage of SWSSC can greatly reduce the consumption of fresh water and river sand, which considerably alleviates the resource shortage problem and environmental burden created by marine infrastructure development. This paper forms part of a large research program currently in progress at Monash University [5-9] in collaboration with The Hong Kong Polytechnic University, Southeast University and Harbin Institute of Technology. To facilitate the application of concrete-filled FRP tubular columns in engineering practice, an accurate theoretical model for predicting their behaviour is required.

The key to predicting the behaviour of concrete-filled FRP tubes is the prediction of response of concrete confined with an FRP tube. It is well understood that the confinement provided by an FRP wrap/tube is passive in nature [10]. Passive confinement refers to situations where the confining pressure increases continuously with the lateral strain of concrete, while active confinement refers to situations where the confining pressure is constant throughout the axial loading process. When the concrete in an FRP wrap (which has negligible longitudinal stiffness/strength) is subjected to axial compression, its lateral expansion is confined by the FRP wrap which is subjected to hoop tension.

The confining pressure increases continuously due to the linear elastic stress-strain behaviour of FRP, which is different from the confinement mechanism of concrete-filled steel tube; in the latter, the confining pressure is reasonably constant after the yielding of steel, so the confinement mechanism is close to that of active confinement. The confinement mechanism of concrete-filled FRP tubes is similar to that of concrete confined with an FRP wrap except that the FRP tube, whose longitudinal stiffness/strength is significant, is in a biaxial stress state. Extensive research [11] has been conducted on FRP-confined circular concrete columns [or simply referred to as “FRP-confined concrete” as the concrete in a circular section is under (nominally) uniform confinement] and many stress-strain models have been proposed. These models are generally classified as design-oriented models, which are in closed-form expressions and are easy to use in design, or analysis-oriented models, which employ an incremental numerical procedure [10, 11]. Analysis-oriented models for FRP-confined concrete, that are more versatile and powerful than design-oriented models, can potentially be applied to concrete confined by any material [12].

Most of the existing analysis-oriented models for FRP-confined concrete [13-20] were based on an active confinement base model, and the model of Mander et al. [21], with or without modifications, has been widely adopted as this base model. It has been commonly assumed that the prior stress-path of the confined concrete does not affect its subsequent stress-strain behaviour. Among the existing analysis-oriented stress-strain models for FRP-confined concrete, only Fam and Rizkalla’s model [15] was developed explicitly for concrete-filled FRP tubes in which the biaxial behaviour of the FRP tube is considered; however, all existing analysis-oriented stress-strain models can be easily adapted to model concrete-filled FRP tubes if the FRP tube does not suffer from local buckling failure.

Based on the authors’ experimental observations [5, 6], the structural behaviour of SWSSC-filled FRP tubes under axial compression is different from that of concrete-filled FRP wraps: (a) the FRP

tube can buckle much earlier than rupture failure due to hoop tension; (b) the dilation behaviour of concrete-filled FRP tubes is affected by the Poisson's effect of FRP tube; and (c) the FRP tube makes a significant contribution to the load-carrying capacity and this contribution should not be ignored. Obviously, as the existing analysis-oriented models for FRP-confined concrete, except Fam and Rizkalla's model [15], were established for ordinary concrete-filled FRP wraps, these models do not account for the factors listed as (a)-(c) in the preceding sentence. Even Fam and Rizkalla's model [15] accounts for only two of the factors, and it does not consider the effect of buckling and post-buckling behaviour of FRP tube. Furthermore, it is found that Fam and Rizkalla's model [15] gives a much lower ultimate load for specimens in the authors' experiments [5, 6] if the biaxial failure envelope suggested in [15] is adopted, resulting in inaccuracy in the predicted load-axial strain curves. Therefore, for this simulation exercise on SWSSC-filled FRP tubes, a suitable model is required, especially when the longitudinal strength and stiffness of the FRP tube are comparable to those in the hoop direction.

This paper presents a theoretical model for the compressive behaviour of SWSSC-filled FRP circular tubes, in which an analysis-oriented stress-axial strain model is employed to depict the behaviour of confined SWSSC. Compared to existing analysis-oriented stress-strain models for FRP-confined concrete, the proposed model features improvements mainly in the following aspects: (a) the analysis-oriented stress-strain model presented in Jiang and Teng [17], which was modified from an earlier model proposed by the same group [12], is adapted to consider the effect of biaxial behaviour of FRP tube on the confinement of core concrete; (b) the occurrence of tube buckling and post-buckling behaviour are represented; (c) the contribution of the FRP tube to the axial load-carrying capacity is included. In developing the theoretical model, it is assumed that the behaviour of SWSSC under confinement is the same as that of ordinary concrete, provided the two concretes have the same compressive strength. The limited existing evidence supports this assumption [7, 22], whose validity

will be assessed as part of the presents study. Finally, the proposed model is verified with the experimental results of the authors and other studies.

## 2. EXPERIMENTAL DATA

An experimental database of concrete-filled FRP tubes under axial compression was employed in the present study to support the development of a theoretical model. This database included 12 specimens with multiple fiber directions (denoted by  $[\pm 15/\pm 45\pm 75]$ , [5, 6]) and 3 specimens with (almost) unidirectional fibers (denoted by  $[\pm 89]$ , newly tested specimens). Seawater and sea sand concrete (SWSSC) of normal strength was used in these specimens. Details of the specimens are summarized in Table 1. The material properties of FRP are summarized in Table 2 and the typical stress-strain curves of FRP in the hoop direction are shown in Fig. 1. The longitudinal compressive strength is much lower than the corresponding tensile strength due mainly to the micro-buckling of fibers. As shown in Fig. 1, the stress-strain curves of FRP tubes with fibers exclusively oriented in the hoop direction (i.e.  $89^\circ$ ) show pure linearity, while slight nonlinearity is observed for FRP tubes with multiple fiber directions. The secant modulus, which is the ratio of ultimate stress to ultimate strain, is reported in Table 2. The secant modulus ( $E_{hsec}$ ) is a little lower than the elastic modulus ( $E_h$ ) determined according to ASTM D3039/D3039M-14 [23].

All the specimens failed by FRP tube rupture in the hoop direction, accompanied by a sudden loss of load-carrying capacity. Buckling of FRP tubes with multiple fiber directions under axial compression occurred much earlier than tube rupture, but the specimen could still carry an increasing load after tube buckling. Buckling of the FRP tube caused a small sudden drop of applied load with a loud noise and obvious change of tube appearance. After the first appearance of buckling deformation in an FRP tube, more buckles appeared at different locations and this gradual process lasted until tube rupture (either the first appearance of a buckle or the gradual process of buckle appearance is simply referred

to as “buckling” when such use does not cause confusion). By contrast, tube buckling was not observed for concrete-filled FRP tubes with fibers exclusively oriented in the hoop direction; that is, these specimens behaved similar to concrete confined by an FRP wrap [24-27]. It is worth mentioning that the buckling of FRP tube has not been given much attention in previous studies on concrete-filled FRP tubes as all these studies focussed on FRP tubes having fibers oriented close to the hoop direction. The load-axial strain curves of specimens are shown in Fig. 2, in which the occurrence of the first buckle of an FRP tube is highlighted by a hollow circular symbol. The load-axial strain curves of all the specimens display an ascending bilinear shape, indicating that the concrete was sufficiently confined [28]. As shown in Fig. 2a, the buckling of FRP tube caused a slight drop of applied load. The load drop of GFRP tube specimens is more obvious than that of CFRP and BFRP specimens due to the higher longitudinal strength-to-hoop strength ratio ( $f_{ul,c}/f_{uh}$ ) of 0.63 in comparison to the ratios of 0.28 and 0.34 for CFRP and BFRP tubes respectively. The shapes of load-strain curves are similar for both concrete-filled FRP tubes with multiple fiber directions and those with only hoop fibers. It should be noted that the buckling of FRP (CFRP, GFRP and BFRP) tubes all occurred when the axial strain reached around 0.01 to 0.015. This is true for both unfilled FRP tubes and filled FRP tubes as reported in [5, 6]. For an unfilled FRP tube, once buckling occurs, the load-carrying capacity of the tube reduces rapidly [5, 6]. However, an FRP tube supported by infilled concrete can still carry load even after the occurrence of buckling.

### 3. ANALYSIS-ORIENTED MODEL

#### 3.1 Axial strains

The axial strain is an important variable in an analysis-oriented model. Different methods [27, 29] have been adopted by researchers to measure the axial strain, which can be classified as deformation measurement by LVDTs and strain measurement by strain gauges (SGs). LVDTs can measure the overall deformation over the whole height of a specimen, and the axial strain ( $\epsilon_c$ ) is found as the

deformation divided by the gauge length (e.g. specimen height). The axial strain determined by LVDTs is helpful to evaluate the overall deformation characteristics of a specimen, but it may contain strains caused by tube local buckling. By contrast, strain gauges can measure the “localized” strain ( $\varepsilon_{c,SG}$ ) at a specific location, which is closer to the real strain on the FRP tube. However, the strain gauge is likely to be damaged by tube buckling or the exhaustion of its measurement range during a test. Past studies [5, 27] have indicated that the axial strain determined by LVDTs is larger than that obtained by strain gauges.

In the present study, the axial strain determined by LVDTs is adopted during the validation of the proposed theoretical model. The axial strain determined by strain gauges is used to verify the stresses in the FRP tube and to develop the failure criterion for FRP tube buckling. Therefore, the relationship between the two kinds of axial strain should be clarified. The two axial strain values can be related to each other as follows based on the test results:

$$\varepsilon_{c,SG} = k_1 \varepsilon_c \quad (1)$$

The relationships between axial strains obtained from LVDTs and those from SGs of the tested specimens are shown in Fig. 3, from which the best-fit value for  $k_1$  for the above linear equation can be found:  $k_1 = 0.8$  for SWSSC-filled FRP tubes with multiple fiber directions and 0.9 for tubes with only hoop direction fibers. It should be emphasized that the values for  $k_1$  proposed here are derived from the authors’ experiments [5, 6] and cannot be directly applied to other studies. If the relationship between the axial strains obtained from LVDTs and SGs is not available, the  $k_1$  is conservatively set as 1.0 which may lead to a slight lower prediction for the buckling load of FRP tube.

## 3.2 Dilation properties

### 3.2.1 Existing dilation models

All the analysis-oriented models are built on the consideration of interaction between the external confining FRP wrap/tube and the core concrete, and this interaction can be established via a dilation model (i.e. lateral strain-axial strain relationship). The lateral strain-axial strain curves of both unconfined concrete and actively confined concrete display an exponential shape, with the slope of the second-portion of the curve for FRP-confined concrete remaining stable due to the gradual increase in confining pressure [30-32]. The lateral strain-axial strain relationship has been established via many approaches, either implicitly [13-15, 18, 20, 33] or explicitly [12, 16, 19, 32]. Most of these relationships were derived from tests on concrete confined by an FRP wrap, except for Fam and Rizkalla's model [15], which was derived with consideration of Poisson's effect of the FRP tube.

A comparison of the predictions by some typical dilation models with an experimental lateral strain-axial strain curve of SWSSC-filled FRP tube with fibers exclusively oriented in the hoop direction is shown in Fig. 4. These models exhibit different degrees of accuracy, and Teng et al's dilation model [12] is adopted in the present study due to its accuracy as well as its explicit form and simplicity. Jiang and Teng's study [17] indicated that the accuracy of the predicted stress-strain curve of FRP-confined concrete is not sensitive to the details of the lateral strain-axial strain curve provided the ultimate point is precisely predicted and the overall trend of the curve is well captured. The comparison in Fig. 4 also indicates that the use of seawater and sea sand in casting the test specimens did not significantly change the dilation behaviour of the concrete.

### 3.2.2 Dilation model for concrete in an FRP tube

The major difference between an FRP tube and an FRP wrap is that the FRP tube has substantial strength and stiffness in the longitudinal direction, and as a result, the FRP tube is in a biaxial state

of stresses and is significantly affected by the Poisson's ratio. The dilation curves of SWSSC-filled FRP tubes with the layout of  $[\pm 15/\pm 45/\pm 75]$  (regarded as tubes) and  $[\pm 89]$  (regarded as wraps) are compared in Fig. 5. In this paper perfect deformation compatibility is assumed between the concrete and the FRP tube, the hoop strain ( $\varepsilon_h$ ) in the FRP tube is thus taken to be the same as the lateral strain ( $\varepsilon_{lat}$ ) of the concrete. As shown in Fig. 5, the trends of the curves are similar except the initial portion, in which the concrete-filled FRP tube has a steeper slope due to the higher Poisson's ratio of an FRP tube over an FRP wrap. If the Poisson's ratio of FRP tube is higher than that of concrete, the tube tends to separate from the core concrete before the unstable expansion of concrete and the assumption of  $\varepsilon_h = \varepsilon_{lat}$  may not be correct. However, this inaccuracy during the initial stage does not affect the stress-strain model much as the concrete is not effectively confined during the initial stage. Therefore a dilation model developed for concrete-filled FRP wraps is also suitable for concrete-filled FRP tubes if the Poisson's effect and the biaxial stress state are accounted for in the model.

In the present study, Teng et al's dilation model [12] is combined with equations for the biaxial behaviour of the FRP tube to predict the lateral strain-axial strain relationship of SWSSC-filled FRP tubes. The equations in Teng et al's dilation model are as follows:

$$\frac{\varepsilon_c}{\varepsilon_{co}} = 0.85 \left\{ \left[ 1 + 0.75 \left( \frac{-\varepsilon_{lat}}{\varepsilon_{co}} \right) \right]^{0.7} - \exp \left[ -7 \cdot \left( \frac{-\varepsilon_{lat}}{\varepsilon_{co}} \right) \right] \right\} \cdot \left( 1 + 8 \frac{f_l}{f'_{co}} \right) \quad (2)$$

$$f_l = \frac{\sigma_h t_o}{D_i / 2} \quad (3)$$

$$\sigma_h = E_h \varepsilon_h \quad (4)$$

where  $\varepsilon_{co}$  is  $0.000937 \sqrt[4]{f'_{co}}$  (with  $f'_{co}$  in MPa) as suggested by Popovics [34]. As aforementioned, the FRP tube is in a biaxial stress state and the FRP tube can be approximated as an orthotropic elastic membrane [35]:

$$\begin{Bmatrix} \varepsilon_{c,SG} \\ \varepsilon_h \end{Bmatrix} = \begin{bmatrix} \frac{1}{E_l} & \frac{\nu_h}{E_h} \\ \frac{\nu_l}{E_l} & \frac{1}{E_h} \end{bmatrix} \begin{Bmatrix} \sigma_l \\ \sigma_h \end{Bmatrix} \quad (5)$$

where  $\varepsilon_{c,SG}$  is the local axial strain in the FRP tube ( $=k_1\varepsilon_c$ ) and  $\varepsilon_h$  is the hoop strain in the FRP tube ( $=\varepsilon_{lat}$ ). The hoop stress ( $\sigma_h$ ) in Eq. (5) can be rewritten as:

$$\sigma_h = \frac{E_h(\varepsilon_h - \nu_l k_1 \varepsilon_c)}{1 - \nu_l \nu_h} \quad (6)$$

The hoop strain-axial strain relationship of concrete-filled FRP tube can be established by incorporating Eq. (6) into Eqs. (2-3):

$$\varepsilon_c = \frac{(\Phi - \Phi K \varepsilon_h) \varepsilon_{co}}{1 - \Phi K k_1 \nu_l \varepsilon_{co}} \quad (7)$$

where  $\Phi = 0.85\{[1 + 0.75(\frac{-\varepsilon_h}{\varepsilon_{co}})]^{0.7} - \exp[-7 \cdot (\frac{-\varepsilon_h}{\varepsilon_{co}})]\}$  and  $K = \frac{8}{f'_{co}} \cdot \frac{E_h t_o}{(D_i / 2) \cdot (\nu_l \nu_h - 1)}$ .

An FRP tube can buckle well before tube rupture as observed in the experiments (Section 2). After tube buckling, the longitudinal stiffness of the FRP tube ( $\varepsilon_{c,SG}$ ) is much reduced and Eq. (5) is no longer applicable. Because of the difficulty in accurately determining the “real” axial response of post-buckled FRP tube and the fact that the axial stress in the FRP tube is largely released due to tube buckling, it is assumed that the post-buckled FRP tube behaves as an FRP wrap and Teng et al.’s dilation model [12] can be directly used. In conclusion, Eq. (7) is proposed for SWSSC-filled FRP tubes before tube buckling, and Eq. (2) is adopted as the hoop strain-axial strain relationship after tube buckling. It is further proposed that a horizontal line be used to connect the curves obtained by Eq. (7) and Eq. (2) as shown in Fig. 6 to approximate the transition process. The prediction of the first occurrence of local buckling of FRP tube will be discussed in Section 3.3.1.

Comparisons between the predicted lateral strain-axial strain curves and the experimental curves are shown in Fig. 7, in which the first occurrence of buckling of FRP tube is also marked. In some specimens, the hoop strain gauges were damaged by the buckling of FRP tube and the experimental curves shown end before the ultimate load capacity is reached. As shown in Fig. 7, the predictions are in good agreement with the experimental data, indicating that the proposed dilation model (i.e. Eq. (7)) can be used to form part of a theoretical model for SWSSC-filled FRP tubes under axial compression.

### **3.3 Behaviour of FRP tube**

#### ***3.3.1 Buckling of FRP tube***

Since the FRP tube and the core concrete are subjected to simultaneous axial compression, the FRP tube is in a biaxial stress state (axial compression plus hoop tension). The commonly used failure theories for FRP laminates under combined stresses include the maximum stress theory, the maximum strain theory and the Tsai-Wu theory [36]. Among them, the maximum stress theory ignores the Poisson's effect while the Tsai-Wu theory needs the properties of unidirectional lamina, which are difficult to obtain for FRP tubes. After assessing the suitability of these theories, the maximum strain theory was eventually chosen in the present study due to its simplicity and acceptable accuracy.

Besides the biaxial stress state, the interaction between the FRP tube and the core concrete, which leads to the confining pressure, should also be considered in developing the failure criterion. The experimental results indicated that the buckling strain of FRP tube with in-filled concrete was higher than that of a hollow FRP tube [5, 6]. A factor of  $k_2$  is introduced to account for this beneficial effect that delays the onset of buckling in an FRP tube. Therefore the estimated buckling strain of FRP tube is:

$$\varepsilon_{cb} = \frac{k_2 f_{ul,c}}{k_1 E_t} \quad (8)$$

If the axial strain of specimen reaches  $\varepsilon_{cb}$ , the buckling of FRP tube occurs.

As may be expected, a correlation exists between the confining stiffness ( $\rho_K$ ) and  $k_2$  (Fig. 8), in which  $k_2$  is back-calculated from the experiment results. The confining stiffness is define by Eq. (9), which is adopted from Teng et al. [37]. Eq. (10) is proposed to estimate the beneficial effect of concrete core on tube buckling by a regression analysis of experimental data (Fig. 8). As shown in Eq. (10) and Fig. 8,  $k_2$  is equal to 1 if no concrete exists and an upper limit for  $k_2$  is set to 2 based on the available experimental data.

$$\rho_K = \frac{2E_h t_o}{(f'_{co} / \varepsilon_{co}) D_i} \quad (9)$$

$$k_2 = \begin{cases} 4.12\rho_K + 1, & \text{if } \rho_K \leq 0.226 \\ 2, & \text{if } \rho_K > 0.226 \end{cases} \quad (10)$$

The performance of the above proposed buckling failure criterion in predicting FRP tube buckling is shown in Fig. 9. It is worthwhile to mention that the first occurrence of FRP tube buckling during an experiment is judged from its load-axial strain curve and load-hoop strain curve. FRP tube buckling normally caused a sudden drop of applied load and a dramatic change of strain gauge readings. Fig. 9 indicates that the prediction of tube buckling shows acceptable accuracy given the many complicating factors, including the complex lamination structure, biaxial stress state, interaction between tube and core concrete, and errors introduced in the determination of compressive properties of FRP tube.

### 3.3.2 Rupture of FRP tube

The ultimate condition of concrete-filled FRP tubes is reached when the tube is ruptured by hoop tension. The load corresponding to the ultimate condition the FRP tube is generally the maximum

load a specimen can sustain. A descending type of load-axial strain curve is unlikely to appear due to the relatively large thickness of a filament-wound FRP tube in comparison to the small thickness a FRP wrap can have. Theoretically speaking, the hoop strength of FRP tube can be reduced due to the occurrence of tube buckling under longitudinal compression. However, the experimental results ([5, 6]) indicate that the ratio of rupture strain of concrete-filled FRP tube to the ultimate hoop strain obtained from the split-disk material property tests ranges from 0.91 to 1.26, with the average being 1.06 and COV (coefficient of variation) being 0.13. That is, the hoop rupture strain in a SWSSC-filled FRP tube can even be higher than the rupture strain from a split-disk test. This phenomenon can be attributed to the underestimation of the material hoop rupture strain by a split-disk test due to local bending at the gaps of such a test; for FRP wraps, their hoop rupture strain is commonly known to be significantly lower than that from a flat coupon test [38]. Therefore, the rupture of FRP tube due to hoop tension is deemed to occur when its hoop stress reaches the ultimate hoop strength ( $f_{uh}$ ) from a split-disk test.

### **3.4 Load carried by FRP tube**

A major difference between an FRP tube and an FRP wrap is that the tube possesses substantial strength and stiffness in the longitudinal direction. Fig. 10 summarizes the loads carried by the FRP tube and the core concrete respectively at the first occurrence of buckling and the contribution percentage of FRP tube (the top bar of the bar in Fig. 10). It is assumed that the maximum load carried by an FRP tube is equal to that carried by a corresponding hollow short tube in a material properties test. As shown in Fig. 10, the FRP tube shares a considerable part of the applied load, and its contribution should be accounted for in the theoretical model. The contribution of FRP tube to the load-carrying capacity increases with a decrease in the diameter-to-thickness ratio ( $D_o/t_o$ ) or an increase in the longitudinal compressive strength of FRP ( $f_{ul,c}$ ).

A simplified model is proposed to estimate the load carried by FRP tube as shown in Fig. 11 and Eqs. (11-12). It is assumed that the maximum load the FRP tube can carry is equal to the strength of a corresponding hollow short tube ( $N_{fu}$ ). As discussed in Section 3.3.1, the buckling strain of an FRP tube filled with concrete is higher than that of a hollow short tube due to the beneficial effect of in-filled concrete. This assumption is thus generally conservative. Upon the buckling of FRP tube, a certain percentage of the load carried by the FRP tube is released as indicated by the load drop seen in the experimental load-axial strain curves (Fig. 2a). The maximum load drop observed for the test specimens is about 40% of  $N_{fu}$ , and the corresponding reduction factor  $\eta$  is conservatively set to be 0.5 in the present study for simplicity. After the first occurrence of FRP tube buckling, it is assumed that the residual strength of FRP tube decreases linearly to zero until tube rupture. It is known that in an analysis-oriented stress-strain model for FRP-confined concrete, the ultimate axial strain ( $\varepsilon_{cu}$ ) is only attained when the ultimate condition of the FRP tube is reached. Therefore, the hoop strain of FRP tube is adopted here to estimate the residual strength of FRP tube after the first occurrence of tube buckling (Eq. (13)).

$$N_f = \begin{cases} \min\{A_f \sigma_l, N_{fu}\}, & \text{if } \varepsilon_c \leq \varepsilon_{cb} \\ (1-\eta)N_{fu}k_3, & \text{if } \varepsilon_c > \varepsilon_{cb} \end{cases} \quad (11)$$

$$N_{fu} = A_f f_{ul,c} \quad (12)$$

$$k_3 = 1 - \frac{\varepsilon_h - \varepsilon_{hb}}{\varepsilon_{hu} - \varepsilon_{hb}} \quad (13)$$

where  $\varepsilon_h$  is the hoop strain of FRP tube,  $\varepsilon_{hb}$  is the hoop strain of FRP tube at tube buckling, and  $\varepsilon_{hu}$  is the ultimate hoop strain of FRP tube.

### 3.5 Load-axial strain model

#### 3.5.1 Stress-strain curve of confined concrete

A study [7] on unconfined SWSSC has demonstrated that its mechanical behaviour is similar to that of normal concrete (denoted as “freshwater river sand concrete” in [7]). Another study [39] has

concluded that the behaviour of FRP-confined SWSSC is similar to that of FRP-confined normal concrete. In the present study, it is assumed that the stress-strain behaviour of SWSSC is similar to that of normal concrete. In most of the existing analysis-oriented stress-strain models for FRP-confined concrete, the axial stress-strain relationship originally proposed by Popovics [34] for actively confined concrete, which was used by Mander et al. [21] for steel-confined concrete, was adopted as part of the active confinement base model. Popovics's model is rewritten as:

$$\sigma_c = \frac{f_{cc}^* (\varepsilon_c / \varepsilon_{cc}^*)^r}{r - 1 + (\varepsilon_c / \varepsilon_{cc}^*)^r} \quad (14)$$

where  $r$  accounts for the brittleness of concrete and was defined by Carreira and Chu [40] as:

$$r = \frac{E_c}{E_c - f_{cc}^* / \varepsilon_{cc}^*} \quad (15)$$

where  $E_c$  is the initial elastic modulus of concrete, which is taken as  $4730\sqrt{f_{co}'}$  (with  $f_{co}'$  in MPa) in according with ACI 318-11 [41].

Two approaches have been widely adopted by researchers to determine the peak stress ( $f_{cc}^*$ ) of concrete at a given confining pressure ( $f_l$ ). One was proposed by Mander et al. [21] based on the “five-parameter” multiaxial failure surface described by William and Warnke [42], which has been by Mirmiran and Shahawy [19], Spoelstra and Monti [20], Fam and Rizkalla [15], Chun and Park [14] and Aire et al. [43]. The other approach is a simple equation of the following form originally proposed by Richart et al. [44]:

$$f_{cc}^* = f_{co}' + kf_l \quad (16)$$

Different values of  $k$  have been proposed by different researchers (e.g. Marques et al. [18], Albanesi et al. [33], and Teng et al. [12]). In the present study, Eq. (16) is adopted to determine the peak stress and  $k$  is set to 3.5 as suggested by Teng et al. [12].

An expression originally proposed by Richart et al. [44] has been most widely used to predict the axial strain ( $\varepsilon_{cc}^*$ ) of confined concrete at peak stress. A modified version of Richart et al.'s equation was proposed by Jiang and Teng [17] to predict  $\varepsilon_{cc}^*$ :

$$\frac{\varepsilon_{cc}^*}{\varepsilon_{co}} = 1 + 17.5 \left( \frac{f_l}{f_c'} \right)^{1.2} \quad (17)$$

Eq. (17) is also adopted in the present study to predict the axial strain at peak stress.

### 3.5.2 Numerical procedure

The proposed model for predicting the axial load-axial strain relationship needs to be implemented for two stages, separated by FRP tube buckling (Fig. 12). Before buckling, the biaxial behaviour of the FRP tube in resisting the applied load is accounted for. After buckling, the FRP tube is approximated an FRP wrap with a zero Poisson's ratio but the residual axial strength of the FRP tube is considered as discussed in Section 3.4. As shown in Fig. 12, a straight line (AB, ab) is adopted to connect the two parts.

An iterative process is needed to develop the load-axial strain curve as summarized below. The hoop strain in the FRP tube can be determined for a given axial strain from the dilation model. The stresses in the FRP tube can then be calculated from the constitutive law (Eq. (5)) and the confining pressure can then be determined. The stress-strain relationship of actively confined concrete at this confining pressure can be predicted, and the axial stress in the concrete at the given axial strain can be found from the stress-strain relationship (Eqs. (14-17)). The loads carried by the FRP tube and the core concrete can then be determined respectively, and the sum of them is the load carried by the column:

$$N = \sigma_l A_c + N_f \quad (18)$$

The above steps are repeated to generate the entire load-axial strain curve until the rupture of the FRP tube. Fig. 13 summarizes the numerical procedure to generate the load-axial strain curve of concrete-filled FRP tube under axial compression. It should be mentioned that in the dilation model (Eq. (2)),

the axial strain is expressed as a function of lateral strain (= hoop strain). For convenience in computation, a hoop strain increment (and hence the current hoop strain) can be first given and then the axial strain can be determined by the dilation model without iterations, as illustrated in Fig. 13. The hoop strain increment ( $\Delta\varepsilon_h^{(i)}$ ) was adopted as a consistent value in the present study, while it also could change values during the iteration to increase the computation efficiency.

## 4. VERIFICATION OF PROPOSED THEORETICAL MODEL

### 4.1 Load-axial strain response

#### 4.1.1 Authors' experiments

Comparisons between the predicted load-axial strain curves and the experimental curves from [5, 6] are shown in Fig. 14. The details of the specimens are listed in Table 1. Generally, the predictions are in close agreement with the experimental data. For specimens with a diameter of 50 mm (i.e. C50-C and B50-C), the predicted curves provide substantially lower values than experimental curves. This can probably be attributed to two reasons: the predicted buckling strain is lower than the experimental value, and the contribution of FRP tube to the load-carrying capacity is significantly underestimated due to the higher fraction of tube area to the total cross-section area. It is noted that these two specimens are relatively small in size (50mm in diameter and 150mm in height), which may also affect the accuracy of prediction (i.e., size effect). **It is worthwhile to note that these two specimens are of a small size that is unlikely to be used in engineering practice.** A small over-estimation is seen for the concrete-filled GFRP tubes (Fig. 14b), especially at the vicinity of tube buckling. The predicted load-axial strain curves for concrete-filled CFRP and BFRP tubes are in close agreement with the experimental curves (Figures 14c and 14d). However, the predicted ultimate capacity and ultimate axial strain are somewhat lower than the corresponding experimental data for concrete-filled CFRP tubes (i.e. C114-C and C165-C). It was found that the tube rupture strain of these specimens is about 25% higher than the rupture strain obtained from the split-disk test, which can explain the

under-estimation of the ultimate condition. Fig. 14 indicates that the accuracy of the proposed model greatly relies on its accuracy in predicting the effect of buckling on the FRP tube.

#### ***4.1.2 Other researchers' experiments***

While a large number of studies have focused on the behaviour of concrete-filled FRP wraps, there have been limited experimental results for concrete-filled FRP tube. Table 3 summarizes some of the available axial compressive experiments (Fam and Rizkalla [45], El Chabib et al. [46] and Mohamed and Masmoudi [47]) on concrete-filled FRP tubes having considerable longitudinal strength and stiffness. The hoop strength-to-longitudinal strength ratio ( $f_{uh}/f_{ul,c}$ ) ranges from 2.45 to 6.48 and the unconfined concrete strength is less than 60 MPa. A close agreement between the predictions and the experimental curves (Fig. 15) further demonstrates the capability of the proposed model in predicting the load-axial strain response of concrete-filled FRP tubes under axial compression. It should be pointed out that the experimental ultimate axial strain (around 0.01) reported in Fam and Rizkalla's [45] is much lower than those (around 0.04 to 0.05) reported in [46, 47] and in Fig. 14 of the current tests. Furthermore, the buckling of FRP tubes occurred at an axial strain around 0.01 in all the tests reported in [46, 47] and Fig. 14. It seems that the tests reported in [45] were terminated once the buckling occurred, i.e., the post-buckling stage was not captured in the tests reported in [45].

#### **4.2 FRP tube buckling**

The predicted FRP tube buckling loads and corresponding experimental results from Li et al. [5, 6] are compared in Fig. 16. The details of the specimens are given in Section 2. Even though there are some scatters in the prediction of buckling strain as shown in Fig. 9, the predictions for the buckling loads of FRP tubes are accurate (Fig. 16). It should be mentioned that the buckling of concrete-filled FRP tubes with a substantial longitudinal stiffness does not appear to have been examined in previous

studies. However, FRP tube buckling was clearly observed in the authors' experiments ([5, 6]), which occurred with a loud sound and obvious change of tube appearance.

### **4.3 Ultimate condition**

The ultimate load and the ultimate axial strain are defined as the load and the axial strain corresponding to the occurrence of FRP tube rupture. In Fig. 17, the predictions of the proposed model are compared with the experimental results from existing studies [5, 6, 45-47]. Close agreement can be seen in Fig. 17, and the predictions for ultimate loads show higher accuracy than predictions for ultimate axial strains, which is commonly seen in predictions for FRP-confined concrete columns (e.g. [12-20]). In the proposed model, both the longitudinal strength and stiffness are ignored when the specimen reaches the ultimate condition. The method adopted to predict the ultimate load and the ultimate strain is same as that in Teng et al.'s model [12].

## **5. CONCLUSIONS**

This paper has presented a theoretical model for the compressive behaviour of FRP tubular columns filled with seawater and sea sand concrete (SWSSC), in which the FRP tube possesses substantial stiffness and strength. The confined concrete in such tubes is depicted using an existing analysis-oriented stress-strain model in combination with a biaxial model for the FRP tube. The effect of local buckling of the FRP tube is given due attention. The following conclusions are made.

(1) Teng et al.'s [12] dilation model (lateral-axial strain relationship) can be used to closely predict the behaviour of SWSSC under FRP tube confinement provided the biaxial behaviour of the FRP tube is properly accounted for. The predictions of this adapted dilation model are in close agreement with available experimental results.

(2) A maximum strain criterion with appropriate improvements has been proposed in this study to predict the first occurrence of local buckling in FRP tubes, which is a likely phenomenon of concrete-filled FRP tubes with substantial longitudinal stiffness. FRP tube buckling is governed by both the material properties of the FRP tube and the interaction between the tube and encased concrete.

(3) The significant contribution of FRP tube to the load-carrying capacity should not be ignored, and a simplified load-axial strain model has been proposed to determine the load carried by the FRP tube throughout the whole loading process.

(4) A two-stage theoretical model has been proposed for concrete-filled FRP tubular stub columns under axial compression. For stage one (before tube buckling), the biaxial behaviour of the FRP tube, including the Poisson's effect, is considered in the model. For stage two (after tube buckling), the concrete-filled FRP tube is assumed to behave as a concrete-filled FRP wrap except that the residual strength of the FRP tube is appropriately considered in the proposed model. The predictions from the proposed model are in close agreement with available experimental results.

## **ACKNOWLEDGEMENT**

The authors wish to acknowledge the financial support provided by the Australian Research Council (ARC) through an ARC Discovery Grant (DP160100739) and The Hong Kong Polytechnic University (Project account code: 1-BBAG) as well as CST composites which supplied the FRP tubes used in the tests. The tests were conducted in the Civil Engineering Laboratory at Monash University. Thanks are also due to Mr. Long Goh and Mr. Jeff Doddrell for their assistance.

## **REFERENCES**

[1] Fam A, Greene R, Rizkalla S. Field applications of concrete-filled FRP tubes for marine piles. Special Publication. 2003;215:161-80.

- [2] Mirmiran A. Stay-in-place FRP form for concrete columns. *Advances in Structural Engineering*. 2003;6:231-41.
- [3] Teng JG. Performance enhancement of structures through the use of fibre-reinforced polymer (FRP) composites. *Proceedings of 23rd Australasian Conference on the Mechanics of Structures and Materials (ACMSM23)*, 2014.
- [4] Teng JG, Yu T, Dai JG, Chen GM. FRP composites in new construction: current status and opportunities. *Proceedings of 7th National Conference on FRP Composites in Infrastructure*, 2011.
- [5] Li YL, Zhao XL, Raman Singh RK, Al-Saadi S. Experimental study on seawater and sea sand concrete filled GFRP and stainless steel tubular stub columns. *Thin-Walled Structures*. 2016;106:390-406.
- [6] Li YL, Zhao XL, Raman Singh RK, Al-Saadi S. Tests on seawater and sea sand concrete-filled CFRP, BFRP and stainless steel tubular stub columns. *Thin-Walled Structures*. 2016;108:163-84.
- [7] Li YL, Zhao XL, Singh Raman RK, Al-Saadi S. Thermal and mechanical properties of alkali-activated slag paste, mortar and concrete utilising seawater and sea sand. *Construction & Building Materials*. 2018;159:704-24.
- [8] Wang Z, Zhao X-L, Xian G, Wu G, Singh Raman RK, Al-Saadi S. Durability study on interlaminar shear behaviour of basalt-, glass- and carbon-fibre reinforced polymer (B/G/CFRP) bars in sea water sea sand concrete environment. *Construction & Building Materials*. 2017;156:985-1004.
- [9] Wang Z, Zhao X-L, Xian G, Wu G, Singh Raman RK, Al-Saadi S et al. Long-term durability of basalt-and glass-fibre reinforced polymer (BFRP/GFRP) bars in seawater and sea sand concrete environment. *Construction and Building Materials*. 2017;139:467-89.
- [10] Teng JG, Lam L. Behavior and modeling of fiber reinforced polymer-confined concrete. *Journal of structural engineering*. 2004;130:1713-23.

- [11] Ozbakkaloglu T, Lim JC, Vincent T. FRP-confined concrete in circular sections: Review and assessment of stress–strain models. *Engineering Structures*. 2013;49:1068-88.
- [12] Teng JG, Huang YL, Lam L, Ye LP. Theoretical model for fiber-reinforced polymer-confined concrete. *Journal of composites for construction*. 2007;11:201-10.
- [13] Binici B. An analytical model for stress–strain behavior of confined concrete. *Engineering structures*. 2005;27:1040-51.
- [14] Chun S, Park H. Load carrying capacity and ductility of RC columns confined by carbon fiber reinforced polymer. *Proc, 3rd Int Conf on Composites in Infrastructure: Univ. of Arizona San Francisco*; 2002.
- [15] Fam AZ, Rizkalla SH. Confinement model for axially loaded concrete confined by circular fiber-reinforced polymer tubes. *Structural Journal*. 2001;98:451-61.
- [16] Harries KA, Kharel G. Behavior and modeling of concrete subject to variable confining pressure. *Materials Journal*. 2002;99:180-9.
- [17] Jiang T, Teng JG. Analysis-oriented stress–strain models for FRP–confined concrete. *Engineering Structures*. 2007;29:2968-86.
- [18] Marques SPC, Marques DCdSC, Lins da Silva J, Cavalcante MAA. Model for analysis of short columns of concrete confined by fiber-reinforced polymer. *Journal of Composites for Construction*. 2004;8:332-40.
- [19] Mirmiran A, Shahawy M. Dilation characteristics of confined concrete. *Mechanics of Cohesive - frictional Materials*. 1997;2:237-49.
- [20] Spoelstra MR, Monti G. FRP-confined concrete model. *Journal of composites for construction*. 1999;3:143-50.
- [21] Mander JB, Priestley MJ, Park R. Theoretical stress-strain model for confined concrete. *Journal of structural engineering*. 1988;114:1804-26.

- [22] Chen GM, He ZB, Jiang T, Chen JF, Teng JG. Axial compression tests on FRP-confined seawater/sea-sand concrete. 6th Asia-Pacific Conference on FRP in Structures2017.
- [23] ASTM. D3039-D3039M-14, Standard test method for tensile properties of polymer matrix composite materials, DOI: 10.1520-D3039-D3039M-14.
- [24] Ozbakkaloglu T, Lim JC. Axial compressive behavior of FRP-confined concrete: Experimental test database and a new design-oriented model. *Composites Part B: Engineering*. 2013;55:607-34.
- [25] Wu G, Lü Z, Wu Z. Strength and ductility of concrete cylinders confined with FRP composites. *Construction and building materials*. 2006;20:134-48.
- [26] Yu T, Zhang B, Teng JG. Unified cyclic stress–strain model for normal and high strength concrete confined with FRP. *Engineering Structures*. 2015;102:189-201.
- [27] Zhang B, Yu T, Teng JG. Behavior of concrete-filled FRP tubes under cyclic axial compression. *Journal of Composites for Construction*. 2014;19:04014060.
- [28] Lam L, Teng JG. Design-oriented stress–strain model for FRP-confined concrete. *Construction and building materials*. 2003;17:471-89.
- [29] Ozbakkaloglu T, Xie T. Geopolymer concrete-filled FRP tubes: Behavior of circular and square columns under axial compression. *Composites Part B: Engineering*. 2016;96:215-30.
- [30] Sfer D, Carol I, Gettu R, Etse G. Study of the behavior of concrete under triaxial compression. *Journal of Engineering Mechanics*. 2002;128:156-63.
- [31] Smith SS, Willam KJ, Gerstle KH, Sture S. Concrete over the top--or, is there life after peak? *Materials Journal*. 1989;86:491-7.
- [32] Lim JC, Ozbakkaloglu T. Lateral strain-to-axial strain relationship of confined concrete. *Journal of Structural Engineering*. 2014;141:04014141.
- [33] Albanesi T, Nuti C, Vanzi I. Closed form constitutive relationship for concrete filled FRP tubes under compression. *Construction and Building Materials*. 2007;21:409-27.

- [34] Popovics S. A numerical approach to the complete stress-strain curve of concrete. *Cement and concrete research*. 1973;3:583-99.
- [35] Xie P, Lin G, Teng JG, Yu T. Modelling of concrete-filled FRP tubes considering nonlinear biaxial tube behavior. 6th Asia-Pacific Conference on FRP in Structures, 2017.
- [36] Daniel IM, Ishai O. *Engineering mechanics of composite materials*. 2nd ed: Oxford university press; 2006.
- [37] Teng JG, Jiang T, Lam L, Luo YZ. Refinement of a design-oriented stress–strain model for FRP-confined concrete. *Journal of Composites for Construction*. 2009;13:269-78.
- [38] Lam L, Teng JG. Ultimate condition of fiber reinforced polymer-confined concrete. *Journal of Composites for Construction*. 2004;8:539-48.
- [39] Chen GM, He ZB, Jiang T, Chen JF, Teng JG. Effects of seawater and sea-sand on the behaviour of FRP-confined concrete. 6th Asia-Pacific Conference on FRP in Structures, 2017.
- [40] Carreira DJ, Chu K-H. Stress-strain relationship for plain concrete in compression. *Journal Proceedings*1985. p. 797-804.
- [41] ACI318-11. Building code requirements for structural concrete and commentary. ACI; 2011.
- [42] William KJ, Warnke EP. Constitutive model for the triaxial behavior of concrete. *International association for bridge and structural engineering proceedings*. 1975;19:1-30.
- [43] Aire C, Gettu R, Casas J, Marques S, Marques D. Concrete laterally confined with fibre-reinforced polymers (FRP): experimental study and theoretical model. *Materiales de Construcción*. 2010;60:19-31.
- [44] Richart FE, Brandtzaeg A, Brown RL. A study of the failure of concrete under combined compressive stresses. University of Illinois at Urbana Champaign, College of Engineering. Engineering Experiment Station.; 1928.
- [45] Fam A, Rizkalla S. Behavior of axially loaded concrete-filled circular FRP tubes. *A CI Structural J*. 2001;98:280-9.

- [46] El Chabib H, Nehdi M, El Naggari M-H. Behavior of SCC confined in short GFRP tubes. *Cement and Concrete Composites*. 2005;27:55-64.
- [47] Mohamed HM, Masmoudi R. Axial load capacity of concrete-filled FRP tube columns: Experimental versus theoretical predictions. *Journal of composites for construction*. 2010;14:231-43.

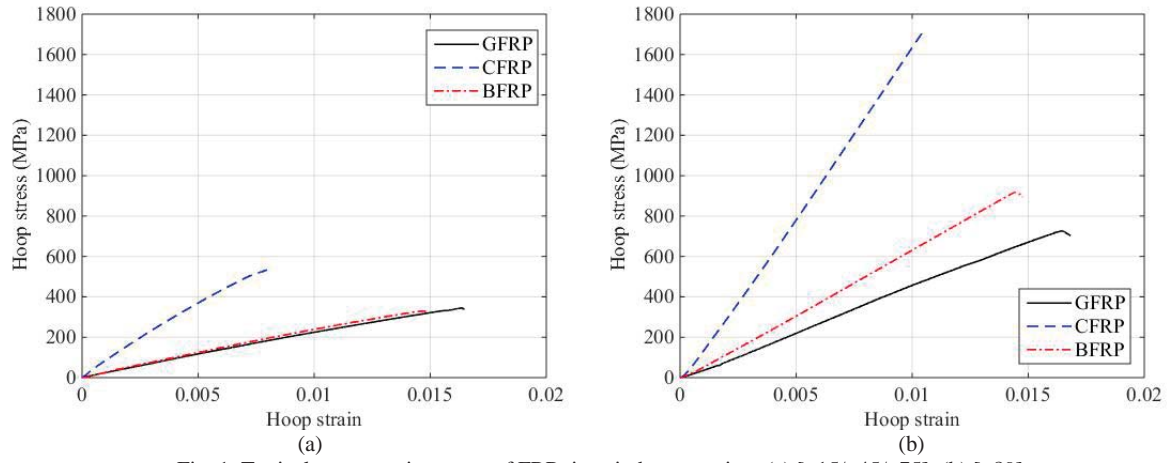


Fig. 1. Typical stress-strain curves of FRP rings in hoop tension: (a)  $[\pm 15/\pm 45/\pm 75]$ ; (b)  $[\pm 89]$ .

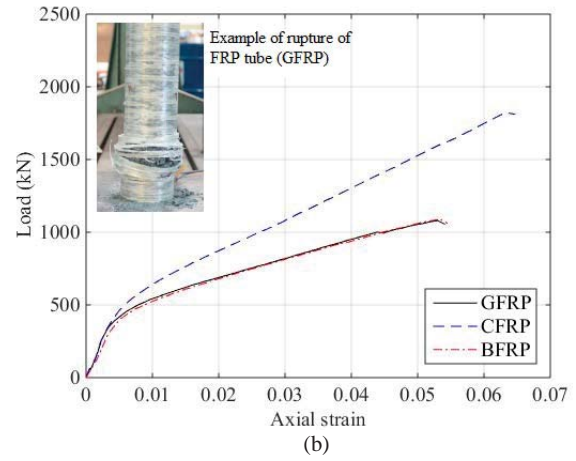
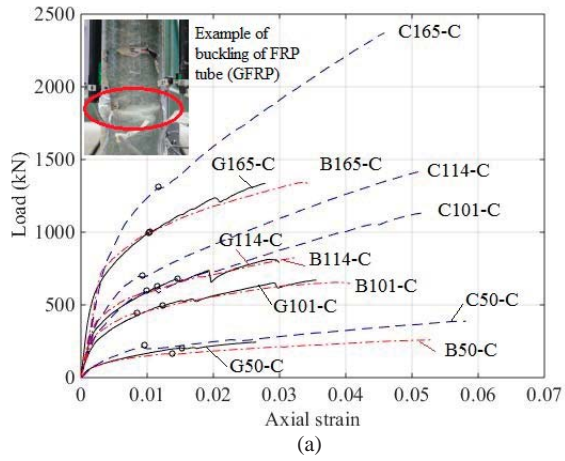


Fig. 2. Load-axial strain curves of SWSSC-filled FRP tubes: (a)  $[\pm 15/\pm 45/\pm 75]$ ; (b)  $[\pm 89]$ .

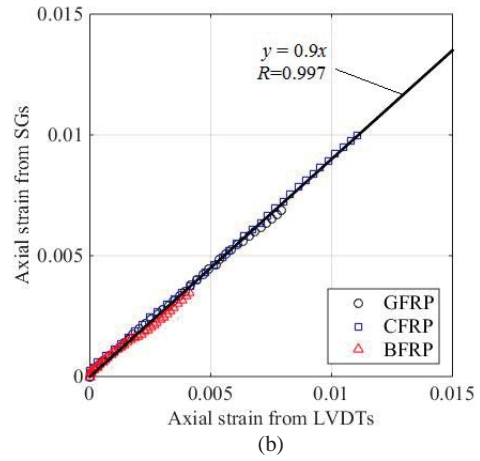
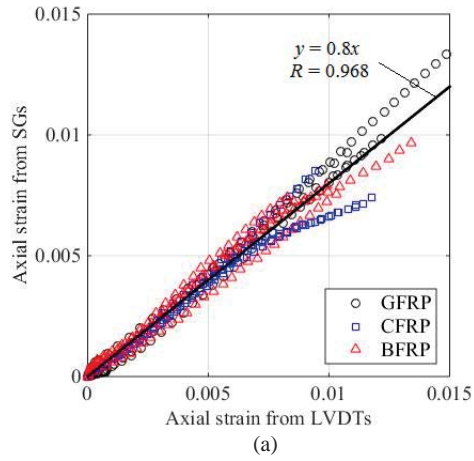
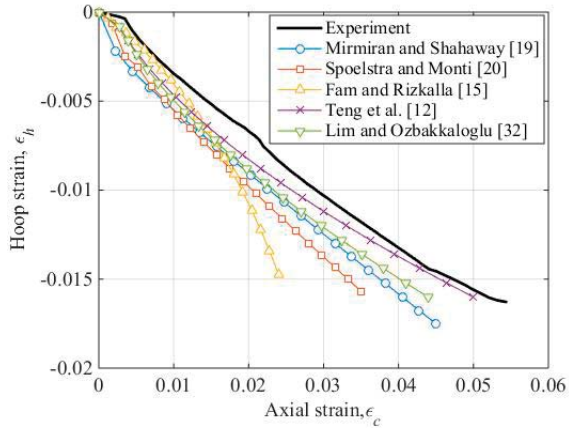
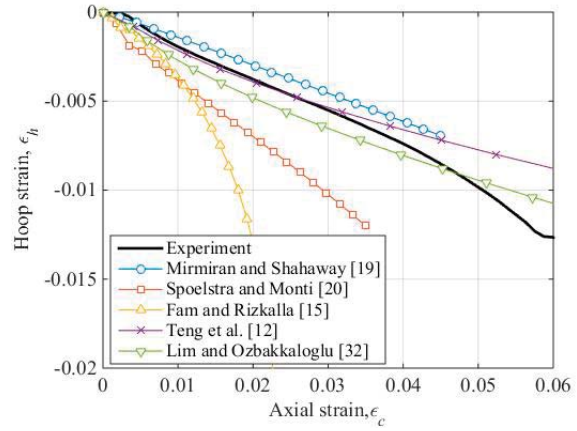


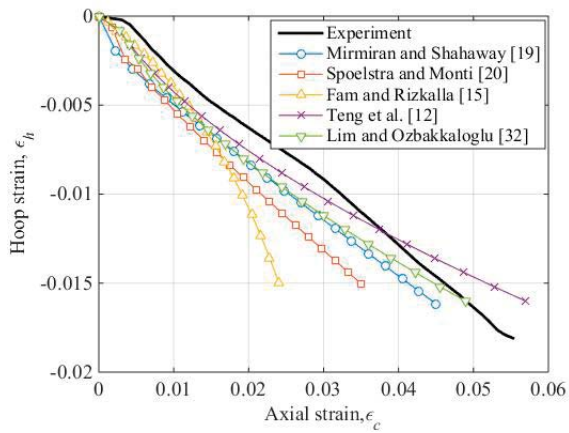
Fig. 3. Comparison of axial strains between LVDTs and strain gauges (SGs): (a)  $[\pm 15/\pm 45/\pm 75]$ ; (b)  $[\pm 89]$ .



(a)



(b)



(c)

Fig. 4. Comparison of model predictions with dilation curve of specimens: (a) G101-89-C; (b) C101-89-C; (c) B101-89-C.

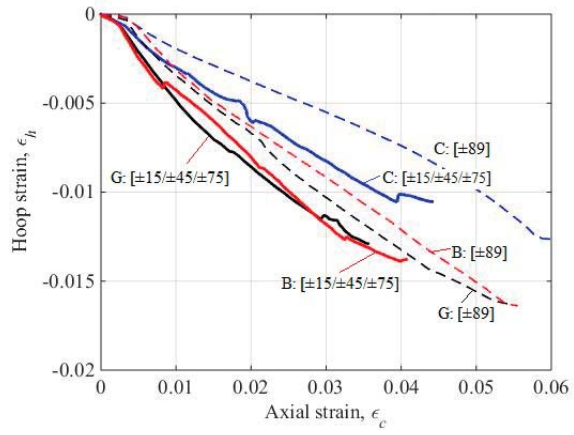


Fig. 5. Dilation curves of concrete-filled FRP tubes and wraps.

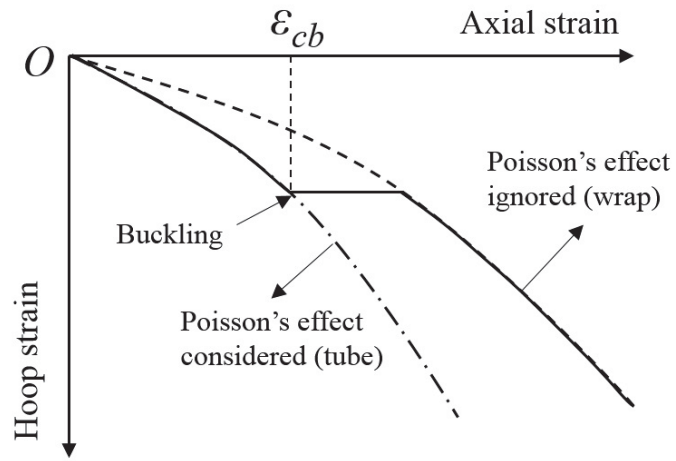
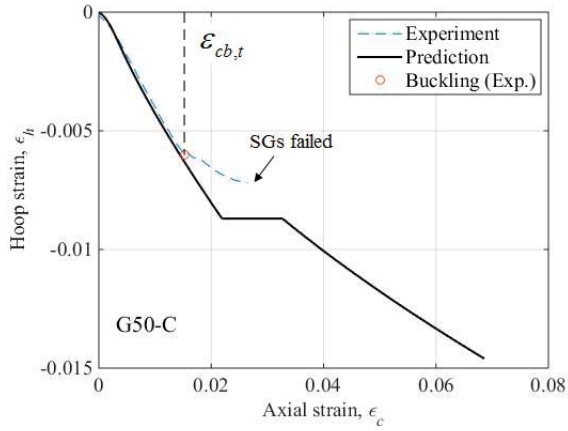
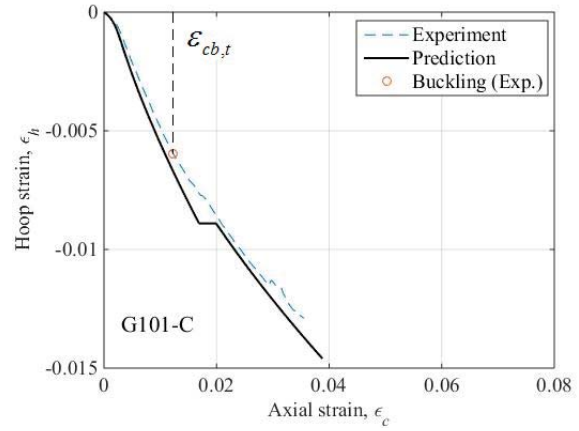


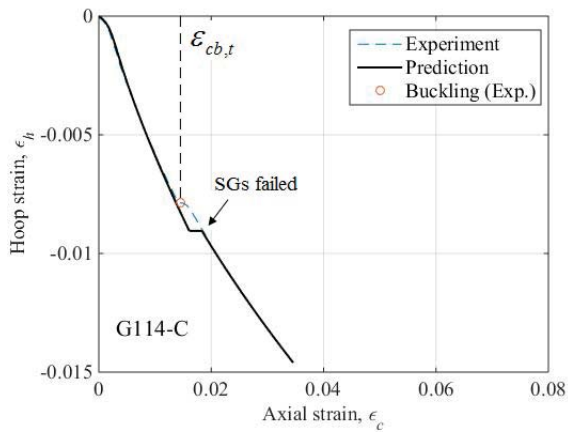
Fig. 6. Conceptual illustration of dilation model for concrete-filled FRP tubes.



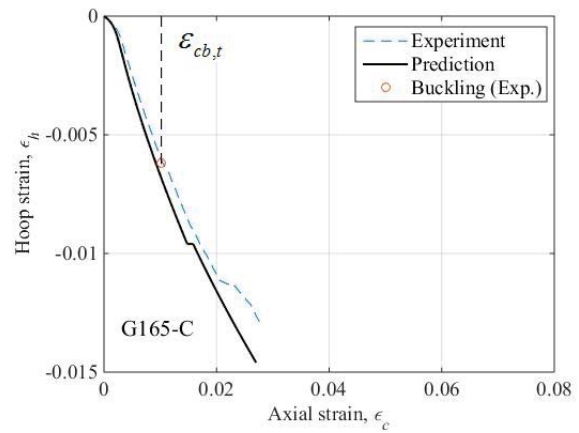
(a) G50-C



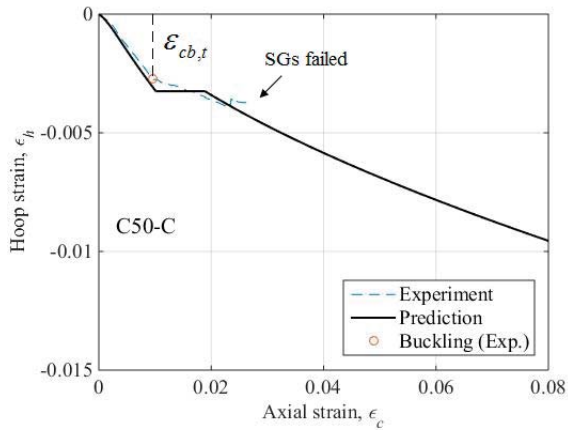
(b) G101-C



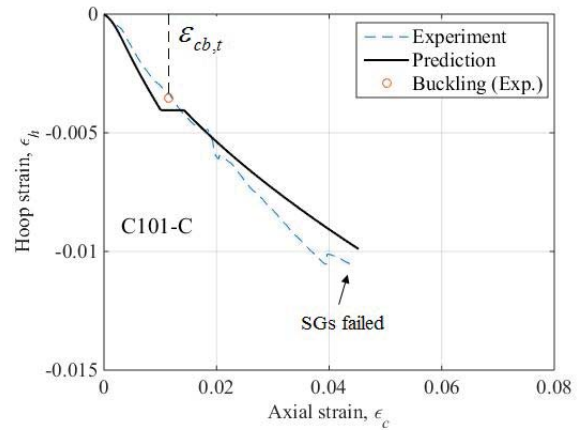
(c) G114-C



(d) G165-C



(e) C50-C



(f) C101-C

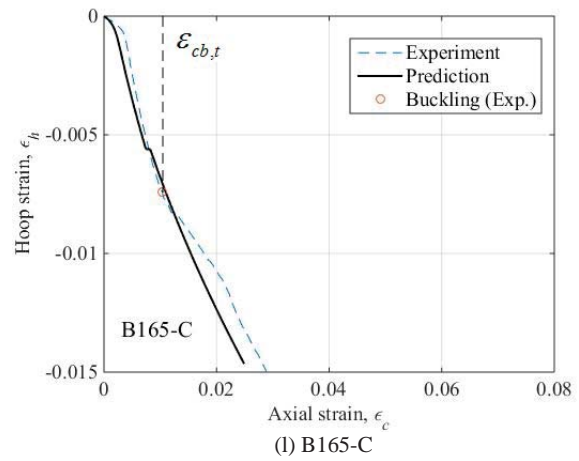
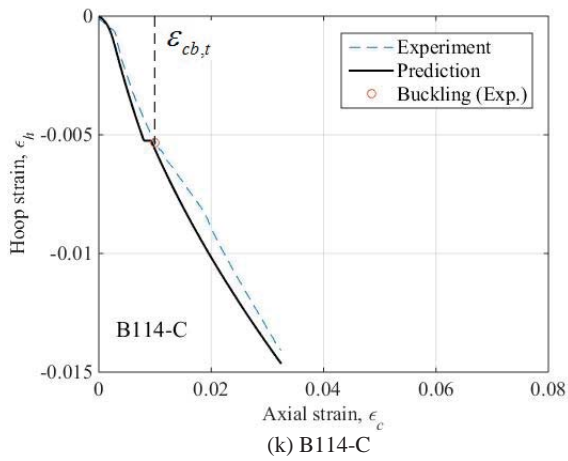
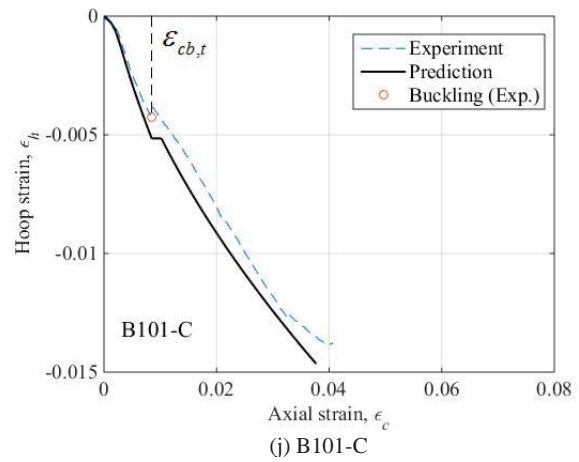
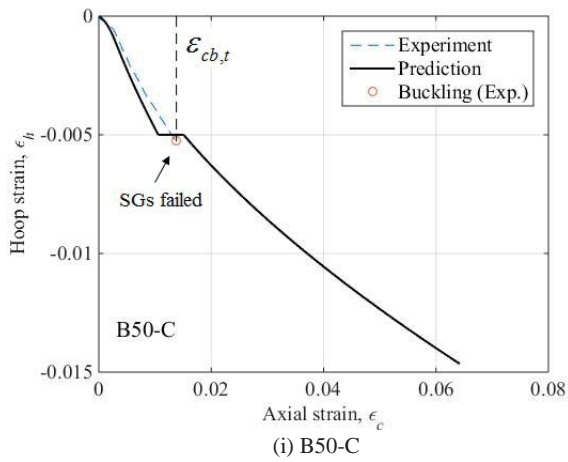
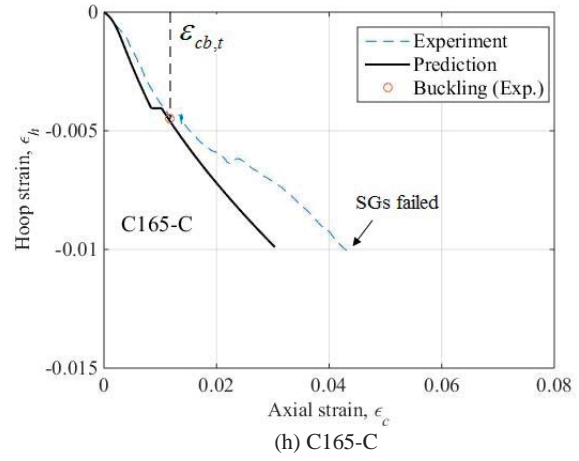
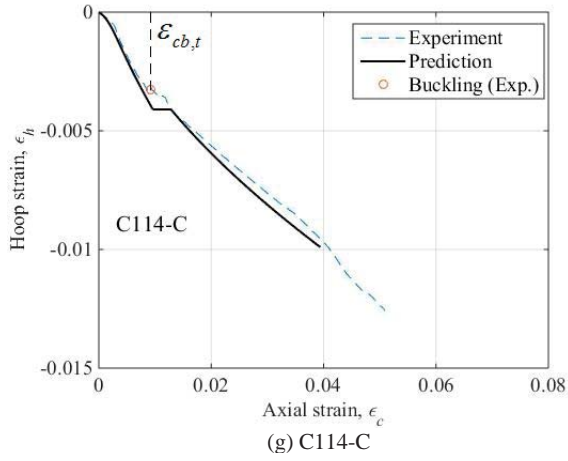


Fig. 7. Verification of dilation model.

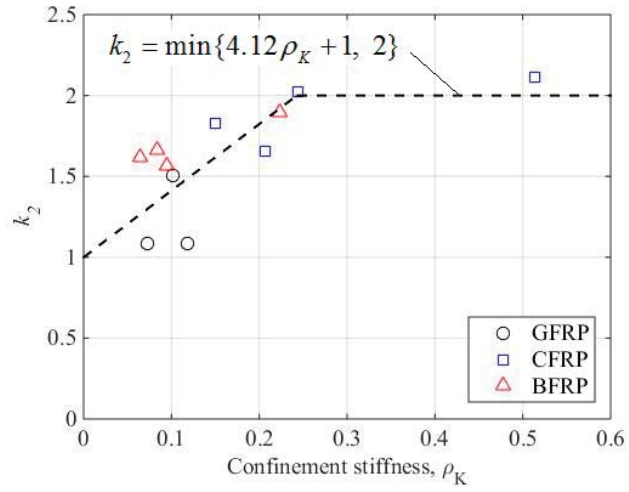


Fig. 8. Determination of the relationship between  $k_2$  and  $\rho_K$ .

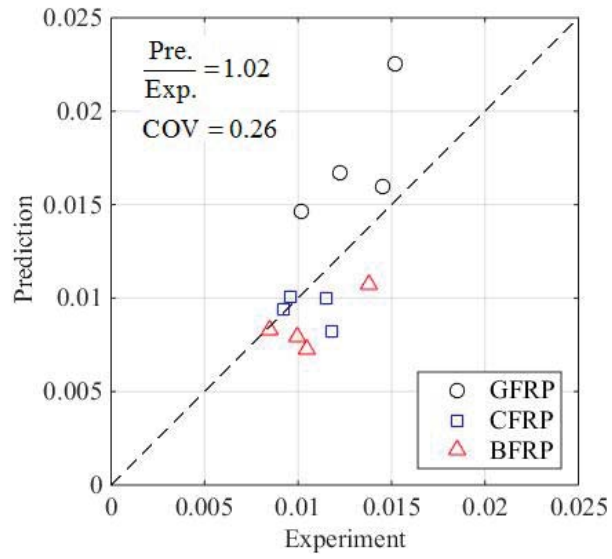


Fig. 9. Axial strain at FRP tube buckling: experiments versus predictions

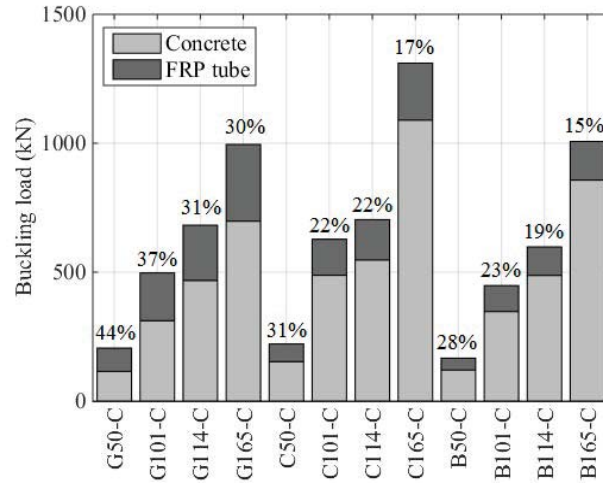


Fig. 10. Percentage contribution of FRP tube to the load-carrying capacity of concrete-filled FRP tube.

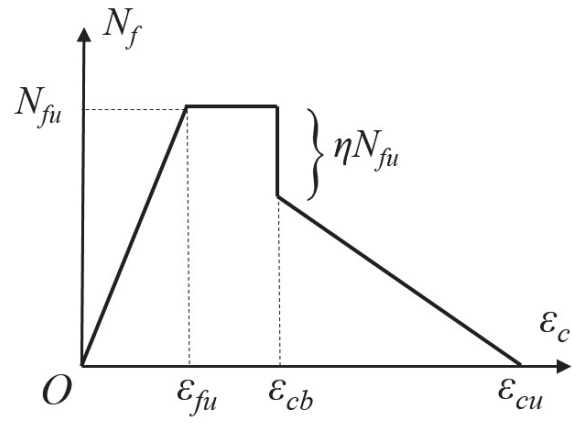


Fig. 11. Simplified load-axial strain model for FRP tube.

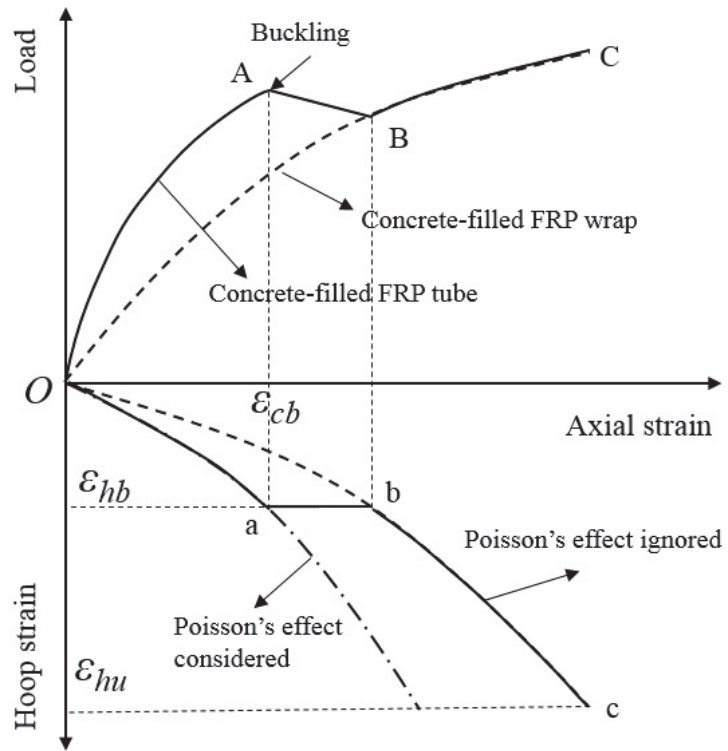


Fig. 12. Conceptual illustration of proposed load-axial strain model.

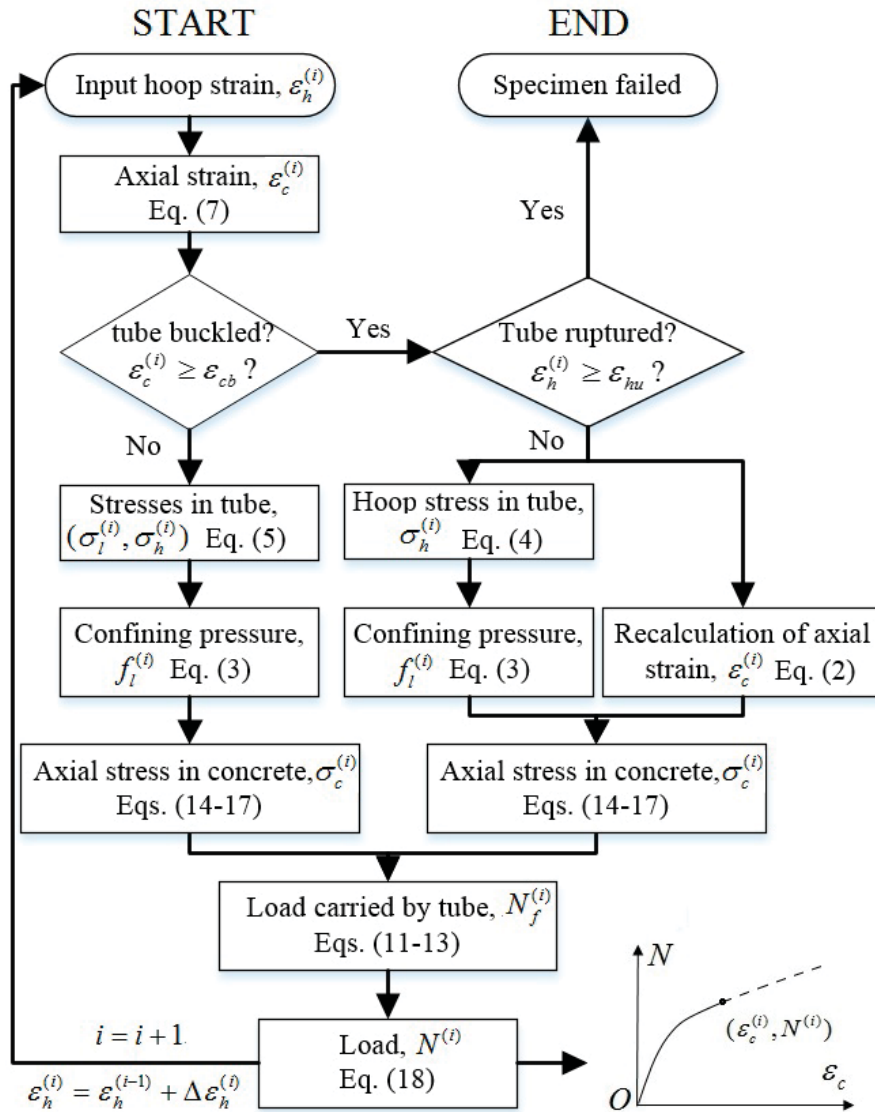


Fig. 13. Flowchart of numerical procedure.

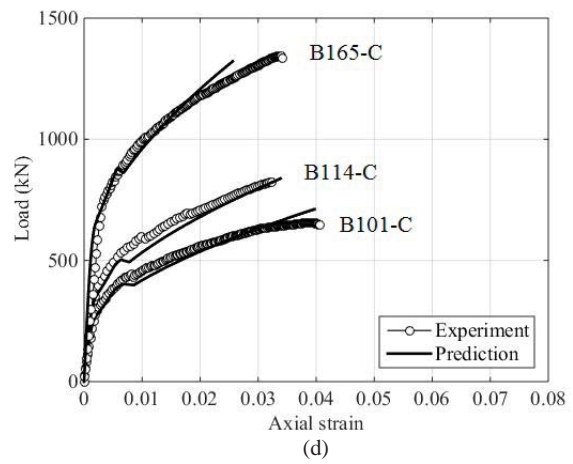
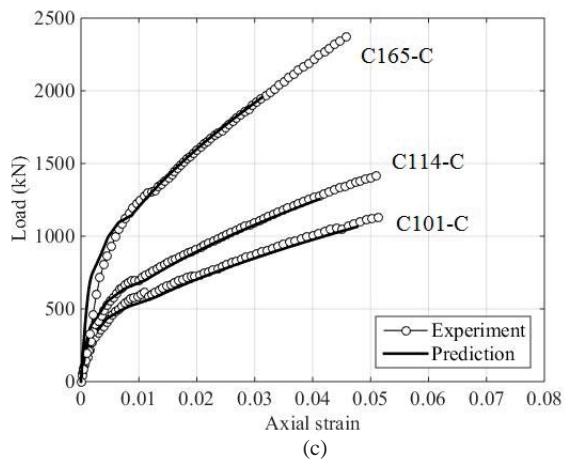
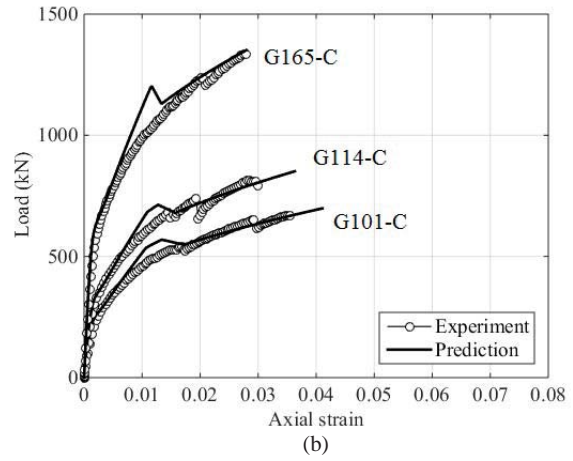
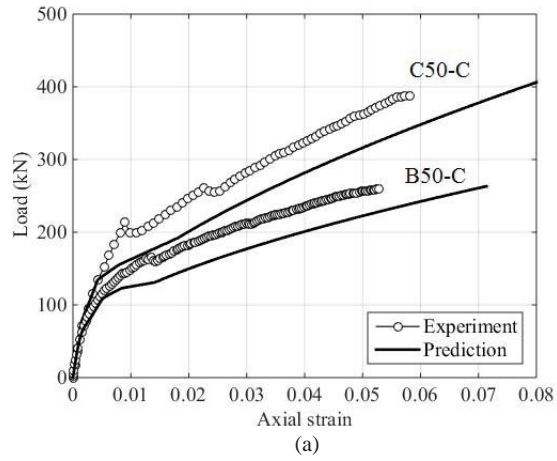


Fig. 14. Comparison of load-axial strain response between predictions and authors' experiments: (a) CFRP and BFRP; (b) GFRP; (c) CFRP (d) BFRP.

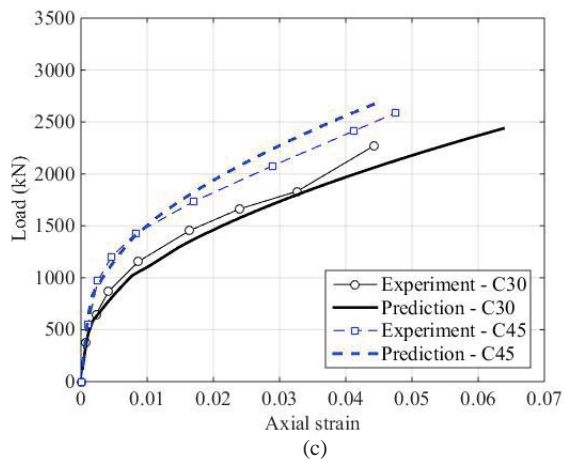
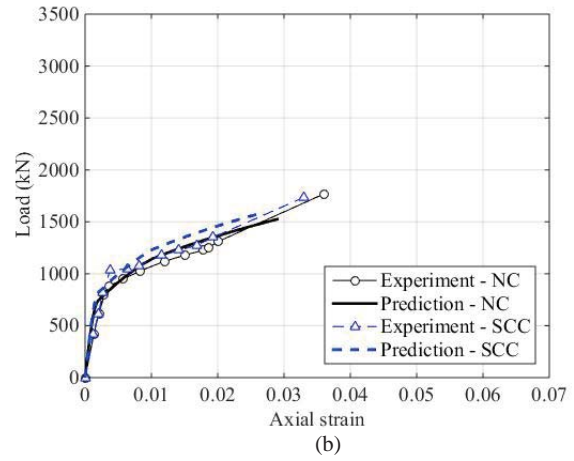
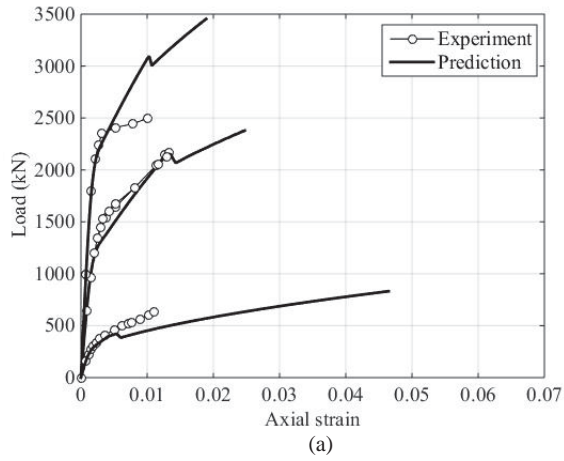


Fig. 15. Comparison of load-axial strain response between predictions and other researchers' experiments: (a) Fam and Rizkalla [45]; (b) El Chabib et al. [46]; (c) Mohamed and Masmoudi [47].

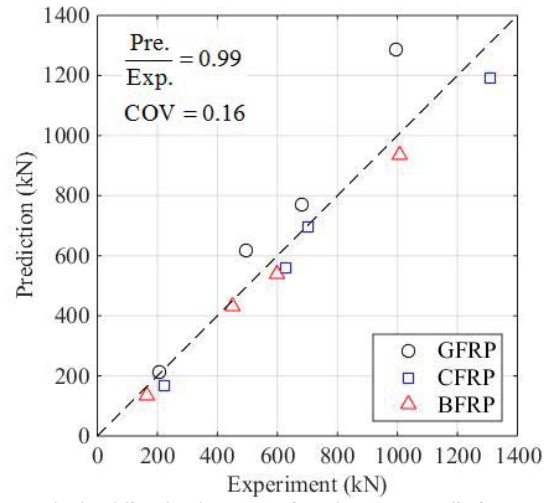


Fig. 16. FRP tube buckling loads: comparison between predictions and experiments.

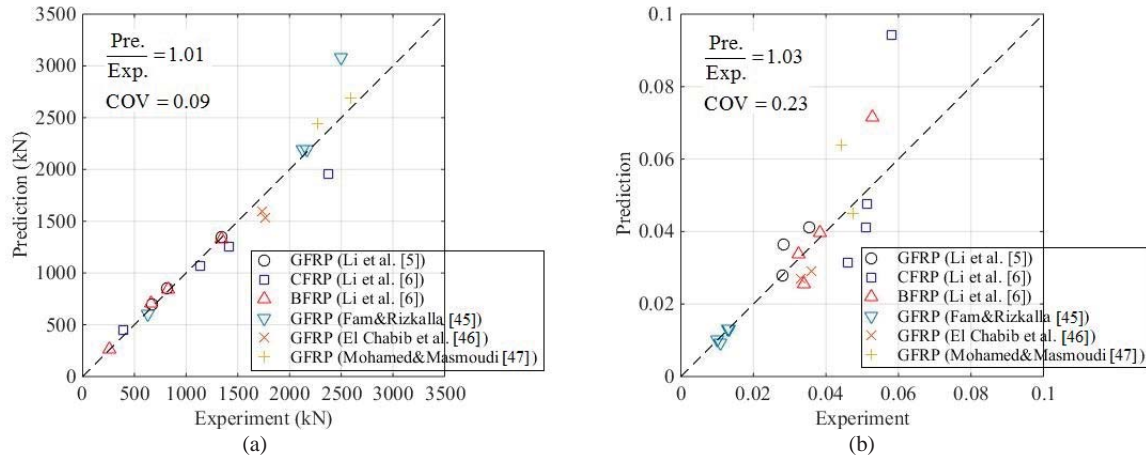


Fig. 17. Comparison of ultimate condition between predictions and experiments: (a) ultimate load; (b) ultimate strain.

Table 1 Specimen details

Specimen	Stacking sequence <sup>a</sup>	FRP type	$D_o$ (mm)	$t_o$ (mm)	$f_{co}'$ (MPa)	$N_t$ (kN)
G50-C	[±15/±45/±75]	GFRP	51.1	3.07	29.8	244
G101-C	[±15/±45/±75]	GFRP	100.1	3.13	29.8	670
G114-C	[±15/±45/±75]	GFRP	115.2	3.13	29.8	813
G165-C	[±15/±45/±75]	GFRP	158.2	3.14	29.8	1336
C50-C	[±15/±45/±75]	CFRP	50.5	2.81	35.8	388
C101-C	[±15/±45/±75]	CFRP	99.9	2.81	35.8	1131
C114-C	[±15/±45/±75]	CFRP	114.6	2.75	35.8	1416
C165-C	[±15/±45/±75]	CFRP	158.1	2.79	35.8	2372
B50-C	[±15/±45/±75]	BFRP	50.0	2.71	32.8	259
B101-C	[±15/±45/±75]	BFRP	100.0	2.92	32.8	656
B114-C	[±15/±45/±75]	BFRP	114.5	2.78	32.8	825
B165-C	[±15/±45/±75]	BFRP	157.7	2.71	32.8	1345
G101-89-C	[±89]	GFRP	98.8	2.17	42.8	1081
C101-89-C	[±89]	CFRP	98.6	2.08	42.8	1837
B101-89-C	[±89]	BFRP	98.4	1.96	42.8	1094

<sup>a</sup>: angles with respect to longitudinal direction (in degrees);

Table 2 Material properties of FRP

Stacking sequence	FRP type	Hoop tension				Axial compression			Axial tension
		$f_{uh}$ (MPa)	$E_h$ (GPa)	$\nu_h$	$E_{hsec}$ (GPa)	$f_{ul,c}$ (MPa)	$E_1$ (GPa)	$\nu_1$	$f_{ul,t}$ (MPa)
[±15/±45/±75]	GFRP	308.8	25.2	0.44	21.1	194.7	21.5	0.27	217.6
	CFRP	592.8	66.7	0.52	59.8	162.9	40.0	0.26	242.9
	BFRP	331.1	24.3	0.30	22.6	113.6	23.9	0.29	124.0
[±89]	GFRP	787.8	49.7	N/A	N/A	61.3	13.6	0.06	N/A
	CFRP	1658.4	162.5	N/A	N/A	99.1	12.2	0.05	N/A
	BFRP	935.5	61.0	N/A	N/A	33.2	23.2	0.11	N/A

Table 3. Specimen details of other researchers' experiments on concrete-filled FRP tubes

Data source	Specimen	Stacking sequence	$D_o$ (mm)	$t_o$ (mm)	$f_{co}'$ (MPa)	Longitudinal direction			Hoop direction			
						$f_{ult}$ (MPa)	$f_{ult,c}$ (MPa)	$E_l$ (GPa)	$\nu_l$	$f_{th}$ (MPa)	$E_h$ (GPa)	$\nu_h$
Fam and Rizkalla [45]	Stub 1	[8/-86/-86/8/-86/8/-85/8/-86]	168.0	2.56 <sup>a</sup>	58.0	282.9	224.1	19.8	0.07	548.0	33.4	0.11
	Stub 2	[8/-86/-86/8/-86/8/-85/8/-86]	168.0	2.56 <sup>a</sup>	58.0	282.9	224.1	19.8	0.07	548.0	33.4	0.11
	Stub 8	[-88/-88/4/-88/-88/4/-88/4/-88]	219.0	2.21 <sup>a</sup>	58.0	201.3	182.6	19.8	0.06	548.0	33.4	0.09
	Stub 11	[-87/3/-87/3/-87/3/-87/3/-87]	100.0	3.08	37.0	444.0	115.0	29.0	0.10 <sup>b</sup>	398.0	23.0	0.08
El Chabib et al. [46]	NC	[±55]	162.0	6.00	39.5	N/A	60.0	8.5	0.39	193.5	10.5	0.48
	SCC <sup>c</sup>	[±55]	162.0	6.00	43.8	N/A	60.0	8.5	0.39	193.5	10.5	0.48
Mohamed & Masmoudi [47]	C30	[±65 <sub>3</sub> /±45/±65 <sub>3</sub> ]	164.8	6.40	30.0	60.2	N/A	9.3	0.29 <sup>b</sup>	390.0	23.6	0.74
	C45	[±65 <sub>3</sub> /±45/±65 <sub>3</sub> ]	164.8	6.40	45.0	60.2	N/A	9.3	0.29 <sup>b</sup>	390.0	23.6	0.74

<sup>a</sup>: excluding the thickness of liner; <sup>b</sup>: calculated by classical laminate theory; <sup>c</sup>: self-compacting concrete.